JOURNAL OF THERMOPHYSICS AND HEAT TRANSFER
Vol. 10, No. 4, October–December 1996

Finite Element Analysis of Poroelastic Composites Undergoing Thermal and Gas Diffusion

Sunpyo Lee*
Kyonggi University, Suwon 440-760, Republic of Korea
Nicholas J. Salamon†
Pennsylvania State University, University Park, Pennsylvania 16802
and
Roy M. Sullivan‡
NASA Marshall Space Flight Center, Huntsville, Alabama 35812

A theory for time-dependent thermal and gas diffusion in mechanically time-rate-independent anisotropic poroelastic composites has been developed. This theory advances previous work by the latter two authors by providing for critical transverse shear through a three-dimensional axisymmetric formulation and using it in a new hypothesis for determining the Biot fluid pressure–solid stress coupling factor. The derived governing equations couple material deformation with temperature and internal pore pressure and more strongly couple gas diffusion and heat transfer than the previous theory. Hence, the theory accounts for the interactions between conductive heat transfer in the porous body and convective heat carried by the mass flux through the pores. The Bubnov Galerkin finite element method is applied to the governing equations to transform them into a semidiscrete finite element system. A numerical procedure is developed to solve the coupled equations in the space and time domains. The method is used to simulate two high-temperature tests involving thermal–chemical decomposition of carbon–phenolic composites. Compared to measured data, the results are accurate. Moreover, unlike previous work, for a single set of poroelastic parameters they are consistent with two measurements in a restrained thermal growth test.

Nomenclature

C_p = heat capacity
c_1 = degree of processing
e_i = elastic strains
e_i^{tot} = total strains
h_g = heat enthalpy
h_R = heat of reaction
K_g = gas bulk modulus
k = permeability matrix
M = Biot's material constant
MW_g = molecular weight
m_g = gas mass increment per unit bulk volume
N_i = elemental shape functions
p = pore pressure
$\boldsymbol{q}$ = heat flux vector
R = universal gas constant
T = absolute temperature
u, w = radial and axial displacement components
v_g = average gas velocity
α_i = Biot's material constants; pressure–stress coupling factors
β_g = thermal expansion coefficient of gas
β_i = thermal expansion coefficients of solid
δ_i = unjacketed compressibilities
ζ = gas volume increment per unit bulk volume
ζ^{tot} = total gas volume increment per unit bulk volume
κ = thermal conductivity matrix
μ = gas viscosity
ρ_g = gas density
ρ_{proc} = density of processed solid
ρ_s = solid density
ρ_{virg} = density of virgin solid
τ_i = total stresses
ϕ = porosity

I. Introduction

POROELASTICITY has been applied to numerous problems in which a fluid, diffusing through a deformable solid, influences the mechanical behavior in a coupled manner. The most common applications involving solid deformation are in geotechnical engineering.[1] Problems coupling fluid diffusion to thermal or electronic diffusion have also been solved within a rigid matrix. Such problems feature two independent field variables, namely, temperature and pressure. Raising the level of complexity to three or more independent field variables, material deformation has been coupled to gas and thermal diffusion in the study of a high-temperature thermal insulation material by Sullivan[2] and Sullivan and Salamon,[3] from which this work is launched, and Weiler.[4]

The theory is founded upon that of Biot,[5] who developed constitutive relations for the elastic behavior of saturated, isotropic porous soils, and Biot and Willis,[6] who expanded them to include anisotropy. Their theory provides a mathematical model for the mechanical behavior of the bulk material by phenomenologically linking the interaction between the solid and fluid phases in the sense of mixtures. Nur and Byerlee[7] discussed the concept of effective stress and defined an effective stress law for isotropic, fluid-filled porous materials. Carroll[8] further developed the effective stress law for anisotropic porous materials and Kurashige[9] reported an anisotropic, thermoelastic formulation. All of these formulations are for treatment of geomaterials.

The class of problems treated here involves an evolutionary process in time during which solid deformation, pore pressure

---

Received July 13, 1995; revision received May 15, 1996; accepted for publication May 16, 1996.

*Lecturer, Department of Mechanical Engineering.

†Professor, Department of Engineering Science and Mechanics, 227 Hammond Building.

‡Aerospace Engineer, Structures and Dynamics Laboratory.

(caused by diffusing gases) and change in temperature in poroelastic bodies interact. In general, the process may involve fluid mass generation associated with conversion of a solid from a virgin state to a processed state driven by a change in energy level in a control volume through which mass and energy flux may transfer. In particular, the present application deals with thermally activated, chemical decomposition of carbon–phenolic composite material used in rocket liners. The theory is more general and may have other applications.

Carbon–phenolic is a polymeric material that chemically decomposes into solid carbon (char) and pyrolysis gases when exposed to high temperature. Initiating at an exposed surface, a char layer forms, governed by chemical reaction kinetics, and advances into the material lagging the thermal front. The solid carbon left behind has a porous structure that permits generated process or decomposition gases to escape. This convective action assisted by a low thermal conductivity of char insulates the interior virgin material from heat. Hence, carbon–phenolic is suitable for high-temperature insulation applications.

This article advances the theory in Refs. 2 and 3 by 1) creating a model for nonuniform, thermal convective fields; 2) developing the coupled, three-dimensional, axisymmetric finite element formulation for anisotropic, axisymmetric structures in a general form; and 3) employing a new empirical, but physical form for Biot's pressure–stress coupling factor. It then uses this formulation to simulate two high-temperature tests done by Stokes,[10] and, after determining a consistent set of poroelastic parameters, achieves excellent agreement with the test data. The following sections cover the theory and finite element formulation. Both contain new approaches that are applied to experiments on decomposing carbon phenolic specimens.

II. General Theory

The problem is first formulated in a Cartesian frame and then set into cylindrical coordinates (r, θ, and z) such that r is the radius of a cylinder and z is the generator normal to the r, θ plane, where θ is the angle of rotation about z. Axial symmetry is invoked by subjecting all fields $(\cdot)$ to the constraint $\partial(\cdot)/\partial\theta = 0$. The resultant degrees of freedom are displacements u and w in the r and z directions, respectively, pressure p and temperature T.

Material points are occupied by both solid and fluid, overlaid in the sense of mixtures, and constitute the bulk material. The porous solid is material devoid of fluid. Moreover, solid and fluid refer to pure solid and pure fluid material, respectively. Stresses are usually referenced to bulk area, hence, they are termed effective. However any quantity denoted $(\cdot)^s$ pertains to the pure solid; such stresses are referenced to pure solid area. Pressure p is that in the pure fluid, i.e., herein the gas.

Mass flux through the porous solid is assumed to be slow, irrotational flow. Temperature at a material point is assumed common to both the solid and fluid, hence, perfect heat transfer occurs between them in a control volume. Heat transfer occurs as conduction in the solid and as convection by diffusion of the gas.

The theory is formulated to achieve a linear, time-marching solution. Nonlinear expressions that arise are linearized.

A. Constitutive Equations

We consider a linear elastic material with ϕ and stiffness C whose pores are saturated with gas under p, which is taken positive for compression. The small elastic strain in the solid, in terms of total and thermal strains, is $e_i = e_i^{\text{tot}} - \beta_i \Delta T$. Similarly, the elastic pore fluid volume fraction change is $\zeta = \zeta^{\text{tot}} + \phi\beta_g\Delta T$ with a plus sign, because pore fluid is lost under a temperature increase at constant pressure. The semicomplementary form of strain energy W (Ref. 11) is

$$W = \tfrac{1}{2}[C_{ij}e_i e_j - 2\alpha_i e_i p - (1/M)p^2] \tag{1}$$

from which τ_i (solid plus fluid pressure referenced to the bulk area) and ζ^{tot} follow:

$$\tau_i = \frac{\partial W}{\partial e_i} = C_{ij}(e_j^{\text{tot}} - \beta_j \Delta T) - \alpha_i p \tag{2}$$

$$\zeta^{\text{tot}} = -\frac{\partial W}{\partial p} - \phi\beta_g\Delta T = \frac{1}{M}p + \alpha_i(e_i^{\text{tot}} - \beta_i\Delta T) - \phi\beta_g\Delta T \tag{3}$$

where repeated subscripts are summed. Reduced indicial notation, employed to represent tensorial quantities, will be defined subsequently.

In Eq. (3), the coefficient M is determined through the isothermal unjacketed test,[6] and can be expressed in terms of Biot's coefficients α_i and compressibilities δ_i as

$$M = \frac{K_g}{\phi - \phi(\delta_1 + \delta_2 + \delta_3)K_g + \alpha_i\delta_i K_g} \tag{4}$$

where $K_g = -V(\partial p/\partial V)_T$ is at a constant temperature taken positive for decreasing volume under compression. For an ideal gas, $K_g \sim p$ and the last term in Eq. (3) varies as $\Delta T/T$, which at high temperatures will be small and may be ignored.

The compressibilities may be determined directly from the unjacketed test, or by referring to Ref. 8

$$\delta_i = \sum_{m=1}^{3} S_{im}^s \tag{5}$$

where S^s denotes an elastic compliance of the solid phase material. An alternative method is to first set α_i, then use (see the dissertation by Lee[12])

$$\{\delta_i\} = [C_{ij}]^{-1}(\{1\} - \{\alpha_i\}) \tag{6}$$

where $\{1\}$ is a column matrix with entries $\{1\ 1\ 1\ 0\ 0\ 0\}$. Conversely, given $\{\delta_i\}$, Eq. (6) may be inverted to determine $\{\alpha_i\}$. The alternative route is adopted here because the freedom to determine α from experiment counters uncertainty in the values of the material constants during decomposition. Details are in Ref. 12; a general development in Cartesian coordinates is given by Weiler,[4] and an alternative is given by Kurashige.[9]

Axisymmetric considerations. The most general material that meets the axisymmetric constraint is monoclinic with material symmetry about the r, z plane[12] and is referred to here as r, z symmetric. The elastic stiffness matrix for this material is written (using the notation $1 \equiv rr$, $2 \equiv \theta\theta$, $3 \equiv zz$, $4 \equiv \theta z$, $5 \equiv rz$, and $6 \equiv r\theta$) as

$$[C] = \begin{bmatrix} C_{11} & C_{12} & C_{13} & 0 & C_{15} & 0 \\ & C_{22} & C_{23} & 0 & C_{25} & 0 \\ & & C_{33} & 0 & C_{35} & 0 \\ & & & C_{44} & 0 & C_{46} \\ \text{Sym} & & & & C_{55} & 0 \\ & & & & & C_{66} \end{bmatrix} \tag{7}$$

and the material has $\alpha_4 = \alpha_6 = 0$ and $\beta_4 = \beta_6 = 0$. For this case, the constitutive Eq. (2) becomes

$$\begin{Bmatrix} \tau_1 \\ \tau_2 \\ \tau_3 \\ \tau_4 \\ \tau_5 \\ \tau_6 \end{Bmatrix} = [C] \begin{Bmatrix} e_1^{\text{tot}} - \beta T \\ e_2^{\text{tot}} - \beta T \\ e_3^{\text{tot}} - \beta T \\ e_4^{\text{tot}} \\ e_5^{\text{tot}} - \beta T \\ e_6^{\text{tot}} \end{Bmatrix} - p \begin{Bmatrix} \alpha_1 \\ \alpha_2 \\ \alpha_3 \\ 0 \\ \alpha_5 \\ 0 \end{Bmatrix} \tag{8}$$

where

$$e_1^{\text{tot}} = \frac{\partial u}{\partial r} \quad e_2^{\text{tot}} = \frac{u}{r} \quad e_3^{\text{tot}} = \frac{\partial w}{\partial z} \quad e_5^{\text{tot}} = \frac{\partial u}{\partial z} + \frac{\partial w}{\partial r} \quad e_4^{\text{tot}} = e_6^{\text{tot}} = 0 \tag{9}$$

B. Momentum Equations

In cylindrical coordinates (r, θ, and z), the equations that govern the motion of the porous, fluid-filled material caused from external loads in the absence of body forces and under quasistatic conditions are written as

$$\begin{aligned} &\frac{\partial \tau_1}{\partial r} + \frac{1}{r}\frac{\partial \tau_6}{\partial \theta} + \frac{\partial \tau_5}{\partial z} + \frac{1}{r}(\tau_1 - \tau_2) = 0 \\ &\frac{\partial \tau_6}{\partial r} + \frac{1}{r}\frac{\partial \tau_2}{\partial \theta} + \frac{\partial \tau_4}{\partial z} + \frac{1}{r}(\tau_6 + \tau_4) = 0 \\ &\frac{\partial \tau_5}{\partial r} + \frac{1}{r}\frac{\partial \tau_4}{\partial \theta} + \frac{\partial \tau_3}{\partial z} + \frac{1}{r}\tau_5 = 0 \end{aligned} \tag{10}$$

Axisymmetric case. Under the constraints of axisymmetric conditions ($v = 0$ and $\partial(\cdot)/\partial\theta = 0$), $e_4^{\text{tot}} = e_6^{\text{tot}} = 0$ from Eq. (9), $\tau_4 = \tau_6 = 0$ from Eq. (8), and the second equation in Eq. (10) is automatically satisfied. Then the equations reduce to

$$\begin{aligned} &\frac{\partial \tau_1}{\partial r} + \frac{\partial \tau_5}{\partial z} + \frac{1}{r}(\tau_1 - \tau_2) = 0 \\ &\frac{\partial \tau_5}{\partial r} + \frac{\partial \tau_3}{\partial z} + \frac{1}{r}\tau_5 = 0 \end{aligned} \tag{11}$$

C. Gas Diffusion Equation

The differential equation governing the flow of fluid through the anisotropic porous solid skeleton, derived from the principle of conservation of mass within a control volume, is

$$\frac{\partial m_g}{\partial t} + \nabla \cdot (\rho_g v_g) = \frac{\partial m_g^{\text{gen}}}{\partial t} \tag{12}$$

where $m_g^{\text{gen}} > 0$ is the mass generation term ($m_g^{\text{gen}} < 0$ is the mass consumed). On the left-hand side (LHS), the first term is the storage term that represents the time rate of gas mass inside the control volume and the second term is the diffusion term that defines the flux of gas mass crossing the boundaries of the control volume.

We assume ρ_g constant during an incremental change in time. Hence, it is treated as a parameter that is updated at each numerical time step. The incremental change in gas mass per unit bulk volume is obtained by multiplying ζ^{tot} by ρ_g. Therefore,

$$\frac{\partial m_g}{\partial t} = \rho_g \frac{\partial \zeta^{\text{tot}}}{\partial t} \tag{13}$$

Hence, from Eq. (3), the mass storage term is written in terms of pressure, strains, and temperature as

$$\frac{\partial m_g}{\partial t} = \rho_g \left[\frac{1}{M}\frac{\partial p}{\partial t} + \alpha_i \frac{\partial e_i^{\text{tot}}}{\partial t} - (\alpha_i\beta_i + \phi\beta_g)\frac{\partial T}{\partial t}\right] \tag{14}$$

In the second term on the LHS of Eq. (12), the volume average gas velocity components in cylindrical coordinates are expressed by Darcy's law for slow, irrotational flow as

$$v_g = -(1/\mu)k \cdot \nabla p \tag{15}$$

$$k = \begin{bmatrix} k_1 & k_6 & k_5 \\ k_6 & k_2 & k_4 \\ k_5 & k_4 & k_3 \end{bmatrix} \tag{16}$$

where Eq. (16) is the permeability matrix for an anisotropic porous body.

The right-hand side (RHS) of Eq. (12) represents the rate of increase in gas mass per unit bulk volume resulting from some chemical conversion or phase change process, and this is equal to the rate at which the solid phase gives up or takes in mass per unit bulk volume. Mathematically

$$\frac{\partial m_g^{\text{gen}}}{\partial t} = -\frac{\partial \rho_s}{\partial t} \tag{17}$$

where the solid density ρ_s may be expressed as a linear function of c_1 as in Ref. 13, hence,

$$\rho_s = c_1\rho_{\text{virg}} + (1 - c_1)\rho_{\text{proc}} \tag{18}$$

in which c_1 is unity at the virgin stage and zero at the completely processed stage. Expanding Eq. (17) using the chain rule,

$$\frac{\partial m_g^{\text{gen}}}{\partial t} = -\frac{\mathrm{d}\rho_s}{\mathrm{d}c_1}\frac{\mathrm{d}c_1}{\mathrm{d}t} = -(\rho_{\text{virg}} - \rho_{\text{proc}})\frac{\mathrm{d}c_1}{\mathrm{d}t} \tag{19}$$

in which the rate of processing $\mathrm{d}c_1/\mathrm{d}t$ is defined in Sec. IV.A by setting up a series of Arrhenius kinetic reaction equations based on experimental data.

Substituting Eqs. (14–16) and (19) into Eq. (12) gives

$$\begin{aligned} &\frac{\rho_g}{M}\left(\frac{\partial p}{\partial t}\right) + \rho_g\alpha_i\left(\frac{\partial e_i^{\text{tot}}}{\partial t}\right) - \rho_g(\alpha_i\beta_i + \phi\beta_g)\left(\frac{\partial T}{\partial t}\right) \\ &\quad + (\rho_{\text{virg}} - \rho_{\text{proc}})\left(\frac{\mathrm{d}c_1}{\mathrm{d}t}\right) - \rho_g\nabla\cdot\left(\frac{1}{\mu}k\cdot\nabla p\right) = 0 \end{aligned} \tag{20}$$

where gas density is treated as a constant locally in space. Equation (20) involves temporal and spatial derivatives of the gas pore pressure and accounts for the changes in pore pressure caused by chemical processing, temperature variations, and solid deformations.

Axisymmetric case. The gas diffusion equation (20) is reduced for a monoclinic r, z-symmetric material in cylindrical coordinates to

$$\begin{aligned} &\frac{\rho_g}{M}\left(\frac{\partial p}{\partial t}\right) + \rho_g\frac{\partial}{\partial t}\left[\alpha_1\frac{\partial u}{\partial r} + \alpha_2\frac{u}{r} + \alpha_3\frac{\partial w}{\partial z}\right. \\ &\quad \left. + \alpha_5\left(\frac{\partial w}{\partial r} + \frac{\partial u}{\partial z}\right)\right] - \rho_g(\alpha_1\beta_1 + \alpha_2\beta_2 + \alpha_3\beta_3 + \alpha_5\beta_5 \\ &\quad + \phi\beta_g)\frac{\partial T}{\partial t} + (\rho_{\text{virg}} - \rho_{\text{proc}})\frac{\mathrm{d}c_1}{\mathrm{d}t} - \rho_g\left\{\frac{1}{r}\frac{\partial}{\partial r}\left[r\left(\frac{k_1}{\mu}\frac{\partial p}{\partial r}\right.\right.\right. \\ &\quad \left.\left. + \frac{k_5}{\mu}\frac{\partial p}{\partial z}\right)\right] + \left.\frac{\partial}{\partial z}\left(\frac{k_5}{\mu}\frac{\partial p}{\partial r} + \frac{k_3}{\mu}\frac{\partial p}{\partial z}\right)\right\} = 0 \end{aligned} \tag{21}$$

where the coefficient M is obtained from Eq. (4), $k_4 = k_6 = 0$ for r, z-symmetric monoclinic materials and Eqs. (9) under axisymmetric conditions are employed.

D. Energy Conservation Equation

The equation of energy conservation that governs the balance of energy in a control volume is written as

$$\frac{\partial E}{\partial t} + \nabla \cdot \boldsymbol{q} = \frac{\partial E^{\text{gen}}}{\partial t} \tag{22}$$

where, on the LHS, the first term is the storage term that represents the rate at which energy is stored within the control volume, and the second term is the diffusion term that defines the flux of energy convecting through the control volume, and the RHS represents the rate at which energy is being generated or consumed because of the process.

The rate of the energy stored in the control volume is the sum of the rate of the energy stored in the solid and gas. The first term of Eq. (22) may be expressed as

$$\frac{\partial E}{\partial t} = [(1 - \phi)\rho_s(C_p)_s + \phi\rho_g(C_p)_g]\left(\frac{\partial T}{\partial t}\right) \tag{23}$$

where the subscripts s and g stand for solid and gas, respectively.

The energy diffusion term consists of two contributions: heat conduction in the bulk solid and heat convection carried by the gas flow through the pores:

$$\boldsymbol{q} = \boldsymbol{q}_{\text{cond}} + \boldsymbol{q}_{\text{conv}} \tag{24}$$

The heat conduction term can be written by the Fourier conduction law for anisotropic materials as

$$q_{\text{cond}} = -\kappa \cdot \nabla T \tag{25}$$

where κ is similar in form to Eq. (16). The convective heat flux is h_g times the gas mass flux $\rho_g v_g$, and is written as

$$q_{\text{conv}} = h_g \rho_g v_g \sim (C_p)_g \rho_g v_g T \tag{26}$$

where the final term is valid if the gas is assumed to be ideal. Substituting Eqs. (25) and (26) into Eq. (24) and taking the divergence of the result gives

$$\nabla \cdot \boldsymbol{q} = -\nabla \cdot (\kappa \cdot \nabla T) - \rho_g (C_p)_g \nabla T \cdot \left(\frac{1}{\mu} k \cdot \nabla p\right) - \rho_g h_g \nabla \cdot \left(\frac{1}{\mu} k \cdot \nabla p\right) \tag{27}$$

where the second and first forms of Eq. (26) are operated upon to get the second and third terms, respectively, and Eq. (15) is recalled. The reason for this juggling act is to strengthen coupling between variables, yet, from intuition, circumvent nonlinearities where possible. Notably, the last term does not appear in Ref. 3 because gas velocity was assumed to be locally constant. However, for the problems involving thermal gradients,[12] both of these terms have a significant effect on the process.

The energy density caused by the heat generated in the control volume is expressed by the product of ρ_{virg}, h_R, and the rate of the process $\mathrm{d}c_1/\mathrm{d}t$ as

$$\frac{\partial E^{\text{gen}}}{\partial t} = -\rho_{\text{virg}} h_R \frac{\mathrm{d}c_1}{\mathrm{d}t} \tag{28}$$

Substitution of Eqs. (23), (27), and (28) into Eq. (22) yields

$$[(1 - \phi)\rho_s(C_p)_s + \phi\rho_g(C_p)_g]\frac{\partial T}{\partial t} - \nabla \cdot (\kappa \cdot \nabla T) - \rho_g (C_p)_g \nabla T \cdot \left(\frac{1}{\mu} k \cdot \nabla p\right) - \rho_g h_g \nabla \cdot \left(\frac{1}{\mu} k \cdot \nabla p\right) + \rho_{\text{virg}} h_R \frac{\mathrm{d}c_1}{\mathrm{d}t} = 0 \tag{29}$$

In the energy conservation equation (29), both pressure and temperature are independent variables. The nonlinear term (third term) can be linearized by choosing either pressure or temperature as a variable parameter and this choice is discussed after Eq. (32).

Axisymmetric case. The energy conservation equation (29) for the axisymmetric case in cylindrical coordinates is written as

$$\begin{aligned}
&\frac{\partial}{\partial t}([(1 - \phi)\rho_s(C_p)_s + \phi\rho_g(C_p)_g]T_g) + \rho_{\text{virg}} h_R \frac{\mathrm{d}c_1}{\mathrm{d}t} \\
&\quad - \frac{1}{r}\frac{\partial}{\partial r}\left[r\left(\kappa_1 \frac{\partial T}{\partial r} + \kappa_5 \frac{\partial T}{\partial z}\right)\right] - \frac{\partial}{\partial z}\left(\kappa_5 \frac{\partial T}{\partial r} + \kappa_3 \frac{\partial T}{\partial z}\right) \\
&\quad - \rho_g(C_p)_g\left[\left(\frac{k_1}{\mu}\frac{\partial p}{\partial r} + \frac{k_5}{\mu}\frac{\partial p}{\partial z}\right)\frac{\partial T}{\partial r} + \left(\frac{k_5}{\mu}\frac{\partial p}{\partial r} + \frac{k_3}{\mu}\frac{\partial p}{\partial z}\right)\frac{\partial T}{\partial z}\right] \\
&\quad - \rho_g h_g \left\{\frac{1}{r}\frac{\partial}{\partial r}\left[r\left(\frac{k_1}{\mu}\frac{\partial p}{\partial r} + \frac{k_5}{\mu}\frac{\partial p}{\partial z}\right)\right] + \frac{\partial}{\partial z}\left(\frac{k_5}{\mu}\frac{\partial p}{\partial r} \right.\right. \\
&\quad \left.\left. + \frac{k_3}{\mu}\frac{\partial p}{\partial z}\right)\right\} = 0
\end{aligned} \tag{30}$$

Because this equation employs the final term in Eq. (26), it is restricted by the assumption of an ideal gas.

III. Axisymmetric Finite Element Formulation

The axisymmetric finite element equations are obtained by successively applying the Galerkin method to Eqs. (11), (21), and (30) in the following form:

$$\int_A N_i(\text{LHS\_of\_referenced\_equation}) r \, \mathrm{d}A = 0 \tag{31}$$

where A is the domain in the r, z plane.

The nonlinear, penultimate term in Eq. (30), namely,

$$-\rho_g(C_p)_g\left[\left(\frac{k_1}{\mu}\frac{\partial p}{\partial r} + \frac{k_5}{\mu}\frac{\partial p}{\partial z}\right)\frac{\partial T}{\partial r} + \left(\frac{k_5}{\mu}\frac{\partial p}{\partial r} + \frac{k_3}{\mu}\frac{\partial p}{\partial z}\right)\frac{\partial T}{\partial z}\right] \tag{32}$$

is linearized by choosing the spatial derivatives of temperature as parameters since pressure is a more sensitive factor to the processes studied. Then applying Green's theorem, and integrating Eqs. (31) and (32) by parts,[12] the following matrix equation is obtained:

$$[C]\frac{\mathrm{d}}{\mathrm{d}t}\{a\} + [K]\{a\} = \{F\} \tag{33}$$

where

$$\begin{gathered}
[C] = \begin{bmatrix} 0 & 0 & 0 & 0 \\ 0 & 0 & 0 & 0 \\ C_{pu} & C_{pw} & C_{pp} & C_{pT} \\ 0 & 0 & 0 & C_{TT} \end{bmatrix} \\
[K] = \begin{bmatrix} K_{uu} & K_{uw} & K_{up} & K_{uT} \\ K_{wu} & K_{ww} & K_{wp} & K_{wT} \\ 0 & 0 & K_{pp} & 0 \\ 0 & 0 & K_{Tp} & K_{TT} \end{bmatrix} \\
\{F\} = [F_u \quad F_w \quad F_p \quad F_T] \qquad \{a\} = [u \quad w \quad p \quad T]
\end{gathered} \tag{34}$$

The elements of $[C]$, $[K]$, and $\{F\}$ are explicitly written in the Appendix.

It should be noted that the coupling term K_{Tp} does not appear in Ref. 3. They treat the spatial derivatives of pressure as parameters that cause these terms to be deposited on the diagonal of the $[K]$ matrix rather than in the K_{Tp} term. The preceding formulation results in a more strongly coupled system of equations and is employed here.

For integration over time, the variably weighted Euler numerical method[14] is employed, which leads to

$$[K_{\text{eff}}]^n\{a\}^{n+1} = \{F_{\text{eff}}\}^n \tag{35}$$

where

$$[K_{\text{eff}}]^n = (1/\Delta t^n)[C]^n + \theta[K]^n - \theta[H]^n \tag{36}$$

$$\{F_{\text{eff}}\}^n = \{F\}^n + \left[\frac{1}{\Delta t^n}[C]^n - (1-\theta)[K]^n - \theta[H]^n\right]\{a\}^n \tag{37}$$

and the superscript n denotes the time step. In Eqs. (36) and (37), the matrix $[H]$ may be defined as

$$[H]^n = \left(\frac{\partial\{F\}}{\partial\{a\}}\right)^n \tag{38}$$

For solution by the fully implicit time-integration scheme, the matrix $[H]$ is required. Details of its formulation are given in the dissertation by Lee.[12] Nonzero elements of $[H]$ are given in the Appendix.

In Eq. (35), $[K_{\text{eff}}]^n$ and $\{F_{\text{eff}}\}^n$ are the effective stiffness matrix and effective force vector at time step t_n, respectively. To obtain the material displacements, pore pressure, and temperature at each time step, Eq. (35) is solved for $\{a\}^{n+1}$ simultaneously using a factorization procedure that is a version of Gauss elimination with partial pivoting.[15]

IV. Decomposing Carbon Phenolics

The governing equations for poroelastic material with thermal and gas diffusion provided in Sec. II are applicable to thermochemically decomposing carbon–phenolic. The momentum equations remain the same, but the generation terms in the gas diffusion and the energy conservation equations require further specialization. The objective is to specialize and apply the linearized theory to models of carbon–phenolic material and simulate laboratory tests to demonstrate it and establish poroelastic parameters over a nonlinear decomposition process.

A. Governing Equations

For the mass generation term (19) in the gas diffusion equation (12), the rate of gas mass accumulation is caused by decomposition reactions and, from Ref. 3, is given by

$$\frac{\partial m_g^{\text{gen}}}{\partial t} = -\sum_{i=1}^{N} RF\rho_{\text{virg}}[(W_0)_i - (W_C)_i]\frac{\mathrm{d}(c_1)_i}{\mathrm{d}t} \tag{39}$$

where RF is the weight fraction of the virgin composite that is resin, $(W_0)_i$ is the fractional weight of the resin that undergoes the ith reaction, $(W_C)_i$ is the fractional weight of the resin that is left as a solid residue by the ith reaction, and N is the number of reactions. The rate of charring $\mathrm{d}(c_1)_i/\mathrm{d}t$ is expressed by the Arrhenius kinetic reaction equation

$$\frac{\mathrm{d}(c_1)_i}{\mathrm{d}t} = -A_i^s(c_1)_i^{n_i^s}\exp\left[-\frac{(E_a^s)_i}{RT}\right] \tag{40}$$

where A^s and n^s are the Arrhenius constants and E_a^s is the activation energy for the chemical reaction. These constants for carbon–phenolic are listed in Table 1.

In this work, pyrolysis gases are treated as ideal and ρ_g in the governing equations is obtained by the ideal gas law

$$\rho_g = (MW_g/RT)p \tag{41}$$

The mechanical and thermal properties of dry carbon–phenolic are listed in Table 2.

B. Restrained Thermal Growth and Free Thermal Expansion Tests and Their Finite Element Models

Stokes[10] conducted two high-temperature experiments on cylindrical carbon–phenolic specimens (dry FM5055), fabricated so that the plane of the carbon fabric is perpendicular to the longitudinal axis of the specimen, to determine thermomechanical behavior during chemical decomposition. The restrained thermal growth (RTG) test measured both the stress required to hold the specimens at a constant longitudinal strain and the resulting lateral strain. The free thermal expansion (FTE) test measured the resulting longitudinal strain. The specimens were heated uniformly at a rate of 5.55 K/s (10°F/s),

Table 1 Constants in the decomposition model for dry carbon–phenolic

Reaction number, i	E_a^s, J/mole	A^s, 1/s	n^s	W_0	W_C
1	88,764.4	1.207305×10^{10}	3.5	0.0015	0
2	117,236	4.057500×10^{9}	6.5	0.095	0
3	211,443.5	3.857777×10^{14}	6.5	0.59	0.29
4	272,155	5.583611×10^{15}	3.3	0.3	0.19

RF = 0.3, $h_R = 0$, and $MW_g = 0.03$ kg/mole.

Table 2 Mechanical and thermal properties of dry carbon–phenolic

	Temperature range, K		
Property	$T < 450$	$450 < T < 533$	$T > 533$
E_L	1.517×10^{10} Pa	$-1.412 \times 10^{8}T + 7.87 \times 10^{10}$ Pa	3.447×10^{9} Pa
E_T	1.793×10^{10} Pa	$-1.7449 \times 10^{8}T + 9.645 \times 10^{10}$ Pa	3.447×10^{9} Pa
ν_{TL}	0	$-0.00343T + 1.83819$	0
ν_{LT}	0	$-0.00289T + 1.551$	0
ν_T	0	0	0
Property	Value	Property	Value
β_T	0.000006 m/m-K	b_L	0.000012 m/m-K
$(k_T)_{\text{virg}}/\mu$	5×10^{-21} m^3-s/kg	$(k_L)_{\text{virg}}/\mu$	5×10^{-21} m^3-s/kg
$(k_T)_{\text{char}}/\mu$	5×10^{-13} m^3-s/kg	$(k_L)_{\text{char}}/\mu$	5×10^{-13} m^3-s/kg
ϕ_{virg}	0.02	ϕ_{char}	0.20
ρ_{virg}	1500.0 kg/m	ρ_{char}	1300.0 kg/m^3
$(C_p)_{\text{solid}}$	1400.0 J/kg-K	$(C_p)_{\text{gas}}$	1088.0 J/kg-K
κ_{solid}	1.44 J/m-s-K	κ_{gas}	0.0 J/m-s-K

Table 3 Boundary conditions for the RTG and FTE test simulations

Location	RTG test	FTE test
$r = 0$	$u = \frac{\partial T}{\partial r} = \frac{\partial p}{\partial r} = 0$	$u = \frac{\partial T}{\partial r} = \frac{\partial p}{\partial r} = 0$
$r = a$	$\frac{\partial T}{\partial r} = 0,\ p = 1$ atm	$\frac{\partial T}{\partial r} = 0,\ p = 1$ atm
$z = 0$	$w = \frac{\partial T}{\partial z} = \frac{\partial p}{\partial z} = 0$	$w = \frac{\partial T}{\partial z} = 0,\ p = 1$ atm
$z = b$	$w = \frac{\partial T}{\partial z} = \frac{\partial p}{\partial z} = 0$	$\frac{\partial T}{\partial z} = 0,\ p = 1$ atm

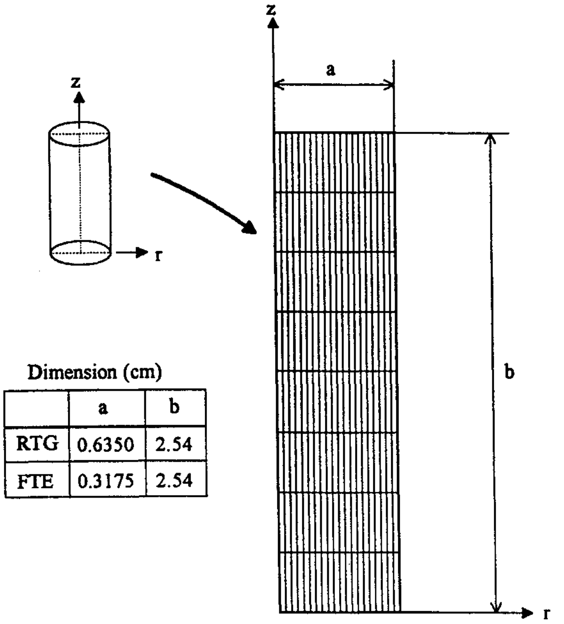

Fig. 1 Finite element mesh for the RTG and FTE test simulations.

and this was controlled using thermocouples embedded in the specimens.

The geometry, coordinate system, and finite element mesh for the RTG and FTE test specimens are shown in Fig. 1. In the RTG test, it was assumed that the end constraints prevent pyrolysis gases from flowing along the axial z direction. Hence, impermeable conditions $\partial p/\partial z = 0$ are prescribed at $z = 0$ and $z = \text{b}$. However, in the FTE test, the pyrolysis gases do flow along the z direction, hence, to allow the gases to escape, atmospheric pressure is specified at $z = 0$ and $z = b$. The initial conditions are $T = 293$ K and $p = 1$ atm in the model and the boundary conditions are summarized in Table 3.

The energy generation term (28) in Eq. (22) is simplified to maintain a uniform temperature increase in the model. An internal heat source is prescribed in each finite element through the integral equation

$$\frac{\partial E^{\text{gen}}}{\partial t} \leftarrow (Q_{\text{int}})_i = \int_A N_i q_{\text{int}} r \, \mathrm{d}A \qquad (42)$$

where q_{int} is the heat generation per unit area, and $(Q_{\text{int}})_i$ is an equivalent nodal value. The value of q_{int}, found by trial and error to achieve the rate of temperature increase of the specimen (5.55 K/s), was determined to be 11.4×10^6 J/m^{3}s.

C. Results for the Pressure–Stress Coupling Factors α

Calculation of the pressure–stress coupling factors from Eqs. (5) and (6) for the virgin elastic composite material requires an experiment, the unjacketed test.[5,6] Unfortunately, such an experiment for carbon–phenolic has not been conducted. Moreover, after decomposition commences, Eqs. (5) and (6) are suspect because of severe changes in material morphology and properties. Hence, further experiments would be desireable. In short, requisite data to calculate these poroelastic parameters do not exist.

Results are obtained by simulating the RTG and FTE tests and varying α, then comparing the material response to experimental data. This was done by physical intuition and trial and error based upon a hypothesis introduced by Lee.[12] This hypothesis assumes 1) isotropic porosity, i.e., $\alpha_i = \alpha$, $i = 1, 2, 3, 5$; 2) a higher proportion of closed pores in virgin material; and 3) increased pore channel opening under high shearing stress action. Consequently, the pressure–stress coupling factor 1) is initially high and, if data are available, can be determined from material properties and Eqs. (5) and (6); 2) decreases as porosity opens, thus inversely as permeability

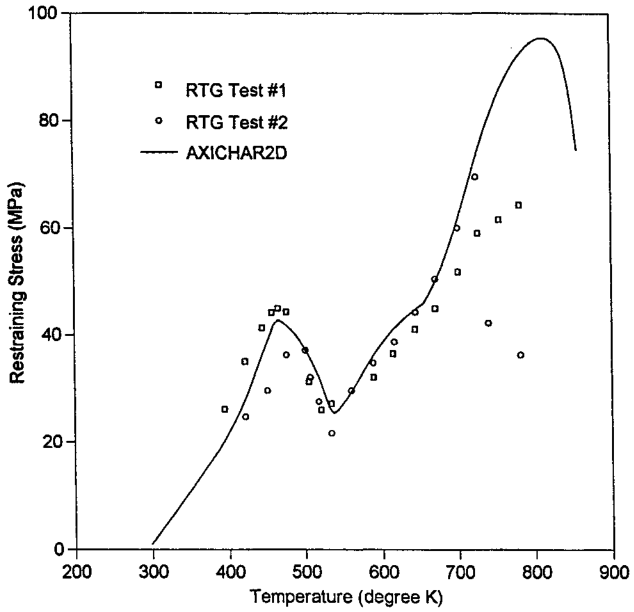

Fig. 2 Restraining stress vs temperature in the RTG test simulation for varying pressure–stress coupling factor.

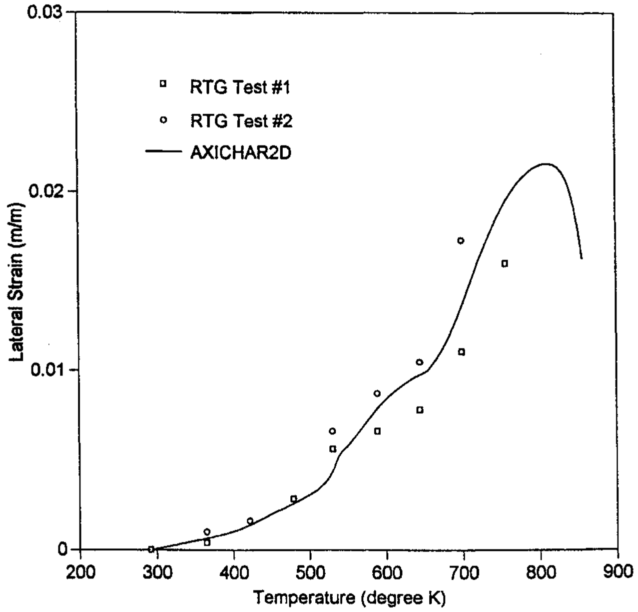

Fig. 3 Lateral strain vs temperature in the RTG test simulation for varying pressure-stress coupling factor.

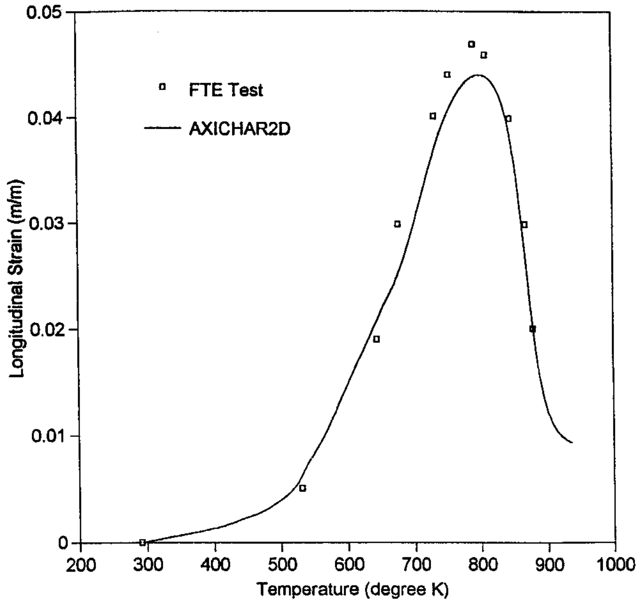

Fig. 4 Longitudinal strain vs temperature in the FTE test simulation for varying pressure–stress coupling factor.

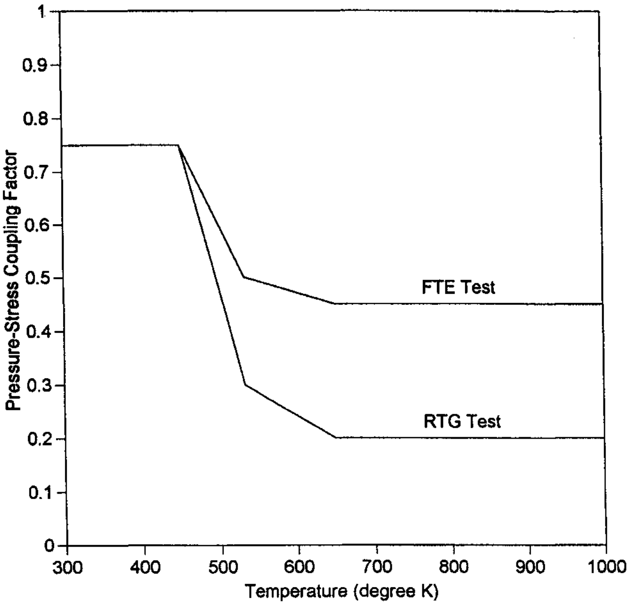

Fig. 5 Typical variation of the pressure–stress coupling factor with temperature for the RTG and FTE test simulations.

increases; and 3) is further decreased if shear stress enhances pore channel growth. [Note: the procedure employed here is to guess α, then use Eqs. (6) and (4) to compute M; hence, α is a curve-fit parameter.]

In Figs. 2 and 3, average restraining stress and average lateral strain of the RTG test simulation are plotted vs average temperature. Also, in Fig. 4, average longitudinal strain of the FTE test simulation is plotted vs average temperature. The variation with temperature of the pressure–stress coupling factor α used in the RTG and FTE simulations, shown in Fig. 5, is that for which the numerical solutions most closely match the measured responses. Only values at corners of the curves were adjusted, those in between corner values were linearly interpolated. The pressure–stress coupling factor for the RTG test simulation was decreased more than that for the FTE test simulation because of a higher shear stress level in the RTG test simulation. Notably for the RTG test simulation, a single choice for the varying pressure–stress coupling factor correlates with data for both restraining stress and lateral strain; Sullivan and Salamon[3] required different constant values to achieve satisfactory results in their parametric study.

V. Conclusions

A coupled set of governing equations for a poroelastic solid with thermal and mass diffusion is derived in a practicable form that requires a minimum of experimental data, yet are sufficiently realistic to entertain engineering problems. In the energy conservation equation, both conductive heat transfer in the bulk solid and convective heat transfer carried by the diffusive gas through the bulk porous solid are treated. The convection terms in which pressure is the independent variable are included in the energy conservation equation so that the convection heat transfer by the diffusive gas is accounted for more accurately than in Ref. 3. These convection terms are coupled with the gas mass diffusion term in the gas diffusion equation, and therefore, pressure appears in both the gas diffusion equation and the energy conservation equation as an independent variable. Hence, the theory now handles the thermal and gas diffusion in the poroelastic solid in a strongly coupled manner.

The material formulation includes the most general anisotropic material under the constraints of axisymmetry, and therefore, permits application to realistic, three-dimensional composite structures. Importantly, the axisymmetric formulation permits accurate computation of the transverse shear stress that is hypothesized to play a significant role in pore channel opening during material decomposition, and in turn, enables finer definition of the pressure–stress coupling factor during decomposition.

The coupled theory, when applied to carbon–phenolic material tests, provides consistent and close correlations with the experimental data using an empirically determined pressure–stress coupling factor suggested by Lee.[12] The improved correlation with experimental data in simulating these tests is attributed to the new formulation for the pressure–stress coupling factor.

It is anticipated that the strong coupling of the equations will play a major role in accurate computation of spatially nonuniform thermal problems such as those encountered in rocket liner structures during firing.

Appendix: Finite Element matrix Entrees

The elements of $[C]$, $[K]$, and $\{F\}$ are

$$\begin{aligned}(K_{uu})_{ij} &= \int_A N_{i,r}\left(C_{11}N_{j,r} + C_{12}\frac{1}{r}N_j + C_{15}N_{j,z}\right) r\,\mathrm{d}A\\ &+ \int_A N_{i,z}\left(C_{15}N_{j,r} + C_{25}\frac{1}{r}N_j + C_{55}N_{j,z}\right) r\,\mathrm{d}A\\ &+ \int_A N_i\left(C_{12}N_{j,r} + C_{22}\frac{1}{r}N_j + C_{25}N_{j,z}\right) \mathrm{d}A \qquad \text{(A1)}\end{aligned}$$

$$\begin{aligned}(K_{uw})_{ij} &= \int_A N_{i,r}(C_{15}N_{j,r} + C_{13}N_{j,z})r\,\mathrm{d}A\\ &+ \int_A N_{i,z}(C_{55}N_{j,r} + C_{35}N_{j,z})r\,\mathrm{d}A\\ &+ \int_A N_i(C_{25}N_{j,r} + C_{23}N_{j,z})\,\mathrm{d}A \qquad \text{(A2)}\end{aligned}$$

$$(K_{up})_{ij} = -\int_A N_{i,r}\alpha_1 N_j r\,\mathrm{d}A - \int_A N_{i,z}\alpha_5 N_j r\,\mathrm{d}A - \int_A N_i\alpha_2 N_j\,\mathrm{d}A \qquad \text{(A3)}$$

$$(K_{uT})_{ij} = -\int_A N_{i,r}Q_1 N_j r\,\mathrm{d}A - \int_A N_{i,z}Q_5 N_j r\,\mathrm{d}A - \int_A N_i Q_2 N_j\,\mathrm{d}A \qquad \text{(A4)}$$

$$(K_{wu})_{ij} = \int_A N_{i,r}\left(C_{15}N_{j,r} + C_{25}\frac{1}{r}N_j + C_{55}N_{j,z}\right) r\,\mathrm{d}A + \int_A N_{i,z}\left(C_{13}N_{j,r} + C_{23}\frac{1}{r}N_j + C_{35}N_{j,z}\right) r\,\mathrm{d}A \tag{A5}$$

$$(K_{ww})_{ij} = \int_A N_{i,r}(C_{55}N_{j,r} + C_{35}N_{j,z})r\,\mathrm{d}A + \int_A N_{i,z}(C_{35}N_{j,r} + C_{33}N_{j,z})r\,\mathrm{d}A \tag{A6}$$

$$(K_{wp})_{ij} = -\int_A N_{i,r}\alpha_5 N_j r\,\mathrm{d}A - \int_A N_{i,z}\alpha_3 N_j r\,\mathrm{d}A \tag{A7}$$

$$(K_{wT})_{ij} = -\int_A N_{i,r}Q_5 N_j r\,\mathrm{d}A - \int_A N_{i,z}Q_3 N_j r\,\mathrm{d}A \tag{A8}$$

$$(K_{pp})_{ij} = \int_A N_{i,r}\rho_g\left(\frac{k_1}{\mu}N_{j,r} + \frac{k_5}{\mu}N_{j,z}\right) r\,\mathrm{d}A + \int_A N_{i,z}\rho_g\left(\frac{k_5}{\mu}N_{j,r} + \frac{k_3}{\mu}N_{j,z}\right) r\,\mathrm{d}A \tag{A9}$$

$$\begin{aligned}(K_{Tp})_{ij} = &-\rho_g(C_p)_g\frac{\partial T}{\partial r}\int_A N_i\left(\frac{k_1}{\mu}N_{j,r} + \frac{k_5}{\mu}N_{j,z}\right) r\,\mathrm{d}A \\ &- \rho_g(C_p)_g\frac{\partial T}{\partial z}\int_A N_i\left(\frac{k_5}{\mu}N_{j,r} + \frac{k_3}{\mu}N_{j,z}\right) r\,\mathrm{d}A \\ &+ \rho_g h_g\int_A N_{i,r}\left(\frac{k_1}{\mu}N_{j,r} + \frac{k_5}{\mu}N_{j,z}\right) r\,\mathrm{d}A \\ &+ \rho_g h_g\int_A N_{i,z}\left(\frac{k_5}{\mu}N_{j,r} + \frac{k_3}{\mu}N_{j,z}\right) r\,\mathrm{d}A\end{aligned} \tag{A10}$$

$$(K_{TT})_{ij} = \int_A N_{i,r}(\kappa_1 N_{j,r} + \kappa_5 N_{j,z})r\,\mathrm{d}A + \int_A N_{i,z}(\kappa_5 N_{j,r} + \kappa_3 N_{j,z})r\,\mathrm{d}A \tag{A11}$$

$$(C_{pu})_{ij} = \int_A N_i\rho_g(\alpha_1 N_{j,r} + \alpha_5 N_{j,z})r\,\mathrm{d}A + \int_A N_i\alpha_2\rho_g N_j\,\mathrm{d}A \tag{A12}$$

$$(C_{pw})_{ij} = \int_A N_i\rho_g(\alpha_5 N_{j,r} + \alpha_3 N_{j,z})r\,\mathrm{d}A \tag{A13}$$

$$(C_{pp})_{ij} = \int_A N_i\frac{\rho_g}{M}N_j r\,\mathrm{d}A \tag{A14}$$

$$(C_{pT})_{ij} = -\int_A N_i\rho_g(\alpha_1\beta_1 + \alpha_2\beta_2 + \alpha_3\beta_3 + \alpha_5\beta_5 + \phi\beta_g)N_j r\,\mathrm{d}A \tag{A15}$$

$$(C_{TT})_{ij} = \int_A N_i[(1 - \phi)\rho_s(C_p)_s + \phi\rho_g(C_p)_g]N_j r\,\mathrm{d}A \tag{A16}$$

$$(F_u)_i = \int_{s_u} N_i t_r^* r\,\mathrm{d}s \tag{A17}$$

$$(F_w)_i = \int_{s_w} N_i t_z^* r\,\mathrm{d}s \tag{A18}$$

$$(F_p)_i = -(\rho_{\mathrm{virg}} - \rho_{\mathrm{proc}})\int_A N_i(\dot{c}_1)r\,\mathrm{d}A - \rho_g\int_{s_p} N_i(v_g^*)_k n_k r\,\mathrm{d}s \tag{A19}$$

$$(F_T)_i = -\rho_{\mathrm{virg}}h_R\int_A N_i\dot{c}_1 r\,\mathrm{d}A - \int_{s_T} N_i(q^*)_k n_k r\,\mathrm{d}s \tag{A20}$$

where

$$\begin{aligned}Q_1 &= C_{11}\beta_1 + C_{12}\beta_2 + C_{13}\beta_3 + C_{15}\beta_5 \\ Q_2 &= C_{12}\beta_1 + C_{22}\beta_2 + C_{23}\beta_3 + C_{25}\beta_5 \\ Q_3 &= C_{13}\beta_1 + C_{23}\beta_2 + C_{33}\beta_3 + C_{35}\beta_5 \\ Q_5 &= C_{15}\beta_1 + C_{25}\beta_2 + C_{35}\beta_3 + C_{55}\beta_5\end{aligned} \tag{A21}$$

and where v_g^* is the volume average gas velocity specified along the external boundary of arc length s_p, q^* is the heat flux specified on s_T, n_i represents components of the outward unit vector normal to the boundaries, and t_r^* and t_z^* represent traction components distributed over the external boundary of arc length s_u and s_w in the r and z directions, respectively.

The $[H]$ matrix is written explicitly as

$$[H] = \begin{bmatrix} 0 & 0 & 0 & 0 \\ 0 & 0 & 0 & 0 \\ 0 & 0 & 0 & H_{pT} \\ 0 & 0 & 0 & H_{TT} \end{bmatrix} \tag{A22}$$

where

$$(H_{pT})_{ij} = -(\rho_{\mathrm{virg}} - \rho_{\mathrm{char}})\int_A \left(\frac{\partial\dot{c}_1}{\partial T}\right) N_i N_j r\,\mathrm{d}A \tag{A23}$$

$$(H_{TT})_{ij} = -\rho_{\mathrm{virg}}h_R\int_A \left(\frac{\partial\dot{c}_1}{\partial T}\right) N_i N_j r\,\mathrm{d}A \tag{A24}$$

Acknowledgments

The first and the second authors are grateful for support through NASA Research Grant NAG8-879. The third author acknowledges support from the NASA Marshall Space Flight Center.

References

[1] Bazant, Z., *Mechanics of Geomaterials*, Wiley, New York, 1985.

[2] Sullivan, R. M., "A Finite Element Model for Thermochemically Decomposing Polymers," Ph.D. Dissertation, Pennsylvania State Univ., University Park, PA, 1990.

[3] Sullivan, R. M., and Salamon, N. J., "A Finite Element Method for the Thermochemical Decomposition of Polymeric Materials—Part I: Theory," *International Journal of Engineering Science*, Vol. 30, No. 4, 1992, pp. 431–441; also "Part II: Carbon Phenolic Composites," ibid, No. 7, pp. 939–951.

[4] Weiler, F. C., "Fully Coupled Thermo- Poro- Elasto Governing Equations," *Computational Mechanics of Porous Materials and Their Thermal Decomposition*, edited by N. J. Salamon and R. M. Sullivan, Applied Mechanics Div. Vol. 136, American Society of Mechanical Engineers, New York, 1992.

[5] Biot, M. A., "General Theory of Three-Dimensional Consolidation," *Journal of Applied Physics*, Vol. 12, Feb. 1941, pp. 155–164.

[6] Biot, M. A., and Willis, D. G., "The Elastic Coefficients of the Theory of Consolidation," *Journal of Applied Mechanics*, Vol. 24, Dec. 1957, pp. 596–601.

[7] Nur, A., and Byerlee, J. D., "An Exact Effective Stress Law for Elastic Deformation of Rock with Fluids," *Journal of Geophysical Research*, Vol. 76, No. 26, 1971, pp. 6414–6419.

[8] Carroll, M. M., "An Effective Stress Law for Anisotropic Elastic

Deformations,'' *Journal of Geophysical Research*, Vol. 84, No. B13, 1979, pp. 7510–7512.

[9]Kurashige, M., ''A Thermoelastic Theory of Fluid-Filled Porous Materials,'' *International Journal of Solids and Structures*, Vol. 25, No. 9, 1989, pp. 1039–1052.

[10]Stokes, E. H., ''The Effect of Moisture on the Mechanical and Thermal Response of FM5055 Carbon Phenolic Composites,'' Southern Research Institute Rept. SRI-EAS-87-1244-6245-6, Southern Research Inst., Birmingham, AL, 1987.

[11]Rudnicki, J. W., ''Effect of Pore Fluid Diffusion on Deformation and Failure of Rock,'' *Mechanics of Geomaterials*, edited by Z. Bazant, Wiley, New York, 1985, pp. 315–347.

[12]Lee, S., ''Coupled Finite Element Analysis of Decomposing Polymeric Composites and Structures with Subsequent Thermal and Gas Diffusion,'' Ph.D. Dissertation, Pennsylvania State Univ., 1993.

[13]Kansa, E. J., Perlee, H. E., and Chaiken, R. F., ''Mathematical Model of Wood Pyrolysis Including Internal Forced Convection,'' *Combustion and Flame*, Vol. 29, Sept. 1977, pp. 311–324.

[14]Celia, M. A., and Gray, W. G., *Numerical Methods for Differential Equations*, Prentice–Hall, Englewood Cliffs, NJ, 1992.

[15]Dongarra, J. J., Moler, C. B., Bunch, J. R., and Stewart, G. W., *LINPACK Users' Guide*, Society for Industrial and Applied Mathematics, 1979.